Inorganic Chemistry
Article

Inorg. Chem. **2011**, *50*, 1723–1732 **1723**
DOI: 10.1021/ic102174b

Solvent Effects and Dynamic Averaging of ^{195}Pt NMR Shielding in Cisplatin Derivatives

Lionel A. Truflandier, Kiplangat Sutter, and Jochen Autschbach*

Department of Chemistry, University at Buffalo State University of New York, Buffalo, New York 14260-3000, United States

Received October 28, 2010

The influences of solvent effects and dynamic averaging on the ^{195}Pt NMR shielding and chemical shifts of cisplatin and three cisplatin derivatives in aqueous solution were computed using explicit and implicit solvation models. Within the density functional theory framework, these simulations were carried out by combining ab initio molecular dynamics (aiMD) simulations for the phase space sampling with all-electron relativistic NMR shielding tensor calculations using the zeroth-order regular approximation. Structural analyses support the presence of a solvent-assisted "inverse" or "anionic" hydration previously observed in similar square-planar transition-metal complexes. Comparisons with computationally less demanding implicit solvent models show that error cancellation is ubiquitous when dealing with liquid-state NMR simulations. After aiMD averaging, the calculated chemical shifts for the four complexes are in good agreement with experiment, with relative deviations between theory and experiment of about 5% on average (1% of the Pt^{II} chemical shift range).

1. Introduction

Since the discovery of its anticancer properties in 1964,[1] cisplatin [*cis*-diamminedichloroplatinum(II)] and cisplatin derivative drugs have proven to be efficient against a broad spectrum of cancers.[2,3] The improvement of their selectivity with respect to tumor cells, and therefore the elimination of severe side effects, remains a source of intensive research.[4] Naturally, the fact that cisplatin, a small heavy-metal complex, is effective against tumors has sparked intense basic research activity on both the experimental and theoretical fronts in order to fully understand its chemical, physical, and biochemical properties.

A better understanding of the action of platinum-based drugs at various levels, i.e., at the atomic or cellular scales, would be of great interest if one wants to improve the effectiveness of their anticancer properties and overcome problems with resistance. At the molecular level, a large number of theoretical works have been dedicated to the study of cisplatin. Many of these works have focused on the investigation of the hydrolysis mechanism taking place in the intracellular media[5] or on the identification of the different steps involved in the formation of platinum−DNA adducts.[6] The theoretical studies also include the development and application of empirical (molecular mechanics, MM) potential-based Monte Carlo (MC) and molecular dynamics (MD)-based methods,[7] allowing one to reach the mesoscale in terms of the investigated time scales and the size of the system. Although MM-based dynamics is likely to

*To whom correspondence should be addressed. E-mail: jochena@buffalo.edu.

(1) Rosenberg, B.; van Camp, L.; Krigas, T. *Nature* **1965**, *205*, 698–699.
(2) Pil, P.; Lippard, S. J.; Bertino, J. R. *Encyclopedia of Cancer*; Academic Press: New York, 2002; pp 525−543.
(3) Belani, C. *Semin. Oncol.* **2004**, *31*, 25–33.
(4) Farrell, N. *Semin. Oncol.* **2004**, *31*, 1–9.
(5) (a) Lopes, J. F.; Rocha, W. R.; Santos, H. F. D.; Almeida, W. B. D. *J. Chem. Phys.* **2008**, *128*, 165103–14. (b) Robertazzi, A.; Platts, J. A. *J. Comput. Chem.* **2004**, *25*, 1060–1067. (c) Burda, J. V.; Zeizinger, M.; Šponer, J.; Leszczynski, J. *J. Chem. Phys.* **2000**, *113*, 2224–2232. (d) Alberto, M. E.; Lucas, M. F. A.; Pavelka, M.; Russo, N. *J. Phys. Chem. B* **2009**, *113*, 14473–14479. (e) Lucas, M. F. A.; Pavelka, M.; Alberto, M. E.; Russo, N. *J. Phys. Chem. B* **2009**, *113*, 831–838. (f) Deubel, D. V. *J. Am. Chem. Soc.* **2006**, *128*, 1654–1663. (g) Zhang, Y.; Guo, Z.; You, X. *J. Am. Chem. Soc.* **2001**, *123*, 9378–9387. (h) Zimmermann, T.; Burda, J. V. *J. Chem. Phys.* **2009**, *131*, 135101. (I) Sarmah, P.; Deka, R. C. *Int. J. Quantum Chem.* **2008**, *108*, 1400–1409. (j) Banerjee, S.; Sengupta, P. S.; Mukherjee, A. K. *Chem. Phys. Lett.* **2010**, *487*, 108–115. (k) Lau, J. K.; Deubel, D. V. *J. Chem. Theory Comput.* **2006**, *2*, 103–106.
(6) (a) Costa, L. A. S.; Hambley, T. W.; Rocha, W. R.; Almeida, W. B. D.; Santos, H. F. D. *Int. J. Quantum Chem.* **2006**, *106*, 2129–2144. (b) Magistrato, A.; Ruggerone, P.; Spiegel, K.; Carloni, P.; Reedijk, J. *J. Phys. Chem. B* **2006**, *110*, 3604–3613. (c) Gkionis, K.; Platts, J. *J. Biol. Inorg. Chem.* **2009**, *14*, 1165–1174. (d) Matsui, T.; Shigeta, Y.; Hirao, K. *J. Phys. Chem. B* **2007**, *111*, 1176–1181. (e) Silva, V. J. D.; Costa, L. A. S.; Santos, H. F. D. *Int. J. Quantum Chem.* **2008**, *108*, 401–414. (f) Gao, Y.; Zhou, L. *Theor. Chem. Acc.* **2009**, *123*, 455–468. (g) Zimmermann, T.; Chval, Z.; Burda, J. V. *J. Phys. Chem. B* **2009**, *113*, 3139–3150. (h) Robertazzi, A.; Platts, J. A. *Chem.—Eur. J.* **2006**, *12*, 5747–5756. (i) Deubel, D. V. *J. Am. Chem. Soc.* **2002**, *124*, 5834–5842. (j) Raber, J.; Zhu, C.; Eriksson, L. A. *J. Phys. Chem. B* **2005**, *109*, 11006–11015.
(7) (a) Lopes, J. F.; de A. Menezes, V. S.; Duarte, H. A.; Rocha, W. R.; Almeida, W. B. D.; Santos, H. F. D. *J. Phys. Chem. B* **2006**, *110*, 12047–12054. (b) Langlet, J.; Bergès, J.; Caillet, J.; Kozelka, J. *Theor. Chem. Acc.* **2000**, *104*, 247–251. (c) Fu, C.; Tian, S. X. *J. Chem. Phys.* **2010**, *132*, 174507. (d) Spiegel, K.; Magistrato, A.; Maurer, P.; Ruggerone, P.; Rothlisberger, U.; Carloni, P.; Reedijk, J.; Klein, M. L. *J. Comput. Chem.* **2008**, *29*, 38–49. (e) Torrico, F.; Pappalardo, R.; Sánchez Marcos, E.; Martínez, J. *Theor. Chem. Acc.* **2006**, *115*, 196–203.

Published on Web 01/04/2011

be sufficiently accurate to describe the platination of DNA and the induced structural distortions,[8] ab initio MD (aiMD) is the method of choice,[9−11] where applicable.

Within the context of the antitumor activity of platinum-containing drugs, multinuclear NMR has played an important role in the resolution of solution structures of the platinum-induced DNA lesions,[12] as well as in the identification of mechanisms related to its binding to DNA.[13] ^{195}Pt is a sensitive spin 1/2 NMR nucleus with a natural abundance of 33.8% and a large chemical shift range above 13000 ppm. For square-planar platinum(II) complexes, the chemical shift range is on the order of 4000 ppm.[14,16] The too low detection limit at sublethal platinum concentrations prevents the observation of NMR signals under physiological conditions.[15,16] However, under in vitro conditions, ^{195}Pt NMR has proven to be a versatile tool to characterize the coordination sphere of platinum drugs and their reaction product studies,[16,17] including reactions with amino acids and nucleotides[18] or model DNA.[19]

The computation of heavy-metal nucleus NMR parameters poses challenges for quantum chemistry,[20−23] in particular when one is interested in accurately predicting the chemical shifts of platinum complexes in solution.[24−32] From a simple static-structure point of view, one has to deal with the large electron count of the systems under investigation. Moreover, calculated NMR parameters are sensitive to essentially all of the approximations made in the computational model. Some of the difficulties associated with the first-principles theory such as the treatment of electron correlation and relativistic effects simultaneously in an efficient manner can be overcome thanks to the development of fast relativistic NMR methods based on density functional theory (DFT),[20] although one has to keep in mind that approximations made in the electronic structure model remain a source of systematic errors. Moreover, the time scale of NMR spectroscopy is slow compared to characteristic molecular or vibrational time scales. Therefore, it is necessary to go beyond static calculations and determine dynamically averaged NMR parameters.[32−34] Further, solvent effects are an important influence. Although the application of continuum models in NMR computations has met with some success (see refs 35 and 36 and references cited therein), there is mounting evidence that for NMR parameters of metal complexes the inclusion of explicit solvent molecules in a dynamical model at the quantum mechanical (QM) level is crucial for obtaining reasonable agreement with experiment without relying too much on error cancellation.[27,32,37−39]

We have recently demonstrated that for anionic platinum-(II) and -(IV) complexes a combination of aiMD and relativistic NMR methods, based on the zeroth-order regular approximation (ZORA) for relativistic effects combined with DFT using generalized gradient approximation (GGA) functionals, allows one to determine aqueous solution ^{195}Pt chemical shifts within 10% deviation from experiment.[32] Beyond this very reasonable agreement "for the better reasons", this previous work has revealed the considerable influence of the solvent upon the ^{195}Pt shielding in terms of (i) the overall magnitude, such as a 570 ppm solvent contribution for $[PtCl_4]^{2-}$, (ii) solvent-induced medium-range effects, considering that for $[PtBr_4]^{2-}$ the ^{195}Pt NMR shielding is acceptably converged for a solvation shell containing at least 15 explicit nearest water molecules, and (iii) system-dependent solvent signatures, i.e., a nontransferability of solvent-induced shielding contributions between different complexes. As a consequence, error compensations that often benefit the computation of chemical shifts cannot always be relied upon unless the complexes have similar electronic structures around the platinum center *and* similar dynamic structures of their solvation shells.

(8) Spiegel, K.; Magistrato, A.; Carloni, P.; Reedijk, J.; Klein, M. L. *J. Phys. Chem. B* **2007**, *111*, 11873–11876.
(9) Beret, E. C.; Pappalardo, R. R.; Marx, D.; Sánchez Marcos, E. *ChemPhysChem* **2009**, *10*, 1044–1052.
(10) Carloni, P.; Sprik, M.; Andreoni, W. *J. Phys. Chem. B* **2000**, *104*, 823–835.
(11) (a) Lau, J. K.; Ensing, B. *Phys. Chem. Chem. Phys.* **2010**. (b) Spiegel, K.; Magistrato, A. *Org. Biomol. Chem.* **2006**, *4*, 2507–2517. (c) Spiegel, K.; Rothlisberger, U.; Carloni, P. *J. Phys. Chem. B* **2004**, *108*, 2699–2707. (d) Beret, E. C.; Provost, K.; Müller, D.; Sánchez Marcos, E. *J. Phys. Chem. B* **2009**, *113*, 12343–12352.
(12) Lukin, M.; de los Santos, C. *Chem. Rev.* **2006**, *106*, 607–686.
(13) (a) Pil, P.; Lippard, S. *Science* **1992**, *256*, 234–237. (b) Yang, D.; van Boom, S. S. G. E.; Reedijk, J.; van Boom, J. H.; Wang, A. H. *Biochemistry* **1995**, *34*, 12912–12920. (c) Marzilli, L. G.; Saad, J. S.; Kuklenyik, Z.; Keating, K. A.; Xu, Y. *J. Am. Chem. Soc.* **2001**, *123*, 2764–2770. (d) Kartalou, M.; Essigmann, J. M. *Mutat. Res.* **2001**, *478*, 1–21. (e) Huang, H.; Zhu, L.; Reid, B. R.; Drobny, G. P.; Hopkins, P. B. *Science* **1995**, *270*, 1842–1845.
(14) Pregosin, P. S. *Transition Metal Nuclear Magnetic Resonance*; Elsevier Publishing Company: New York, 1991.
(15) Jung, Y.; Lippard, S. J. *Chem. Rev.* **2007**, *107*, 1387–1407.
(16) Berners-Price, S.; Ronconi, L.; Sadler, P. *Prog. Nucl. Magn. Reson. Spectrosc.* **2006**, *49*, 65–98.
(17) Still, B. M.; Kumar, P. G. A.; Aldrich-Wright, J. R.; Price, W. S. *Chem. Soc. Rev.* **2007**, *36*, 665–686.
(18) (a) Miller, S. K.; Marzilli, L. G. *Inorg. Chem.* **1985**, *24*, 2421–2425. (b) Norman, R. E.; Ranford, J. D.; Sadler, P. J. *Inorg. Chem.* **1992**, *31*, 877–888. (c) Berners-Price, S. J.; Frey, U.; Ranford, J. D.; Sadler, P. J. *J. Am. Chem. Soc.* **1993**, *115*, 8649–8659. (d) Stefanov, V. E.; Tulub, A. A.; Kutin, A. A. *Int. J. Biol. Macromol.* **1999**, *26*, 161–166. (e) Łakomska, I.; Szyk, E.; Sitkowski, J.; Kozerski, L.; Wietrzyk, J.; Peczyńska, M.; Nasulewicz, A.; Opolski, A. *J. Inorg. Biochem.* **2004**, *98*, 167–172.
(19) (a) Bancroft, D. P.; Lepre, C. A.; Lippard, S. J. *J. Am. Chem. Soc.* **1990**, *112*, 6860–6871. (b) Hartwig, J. F.; Lippard, S. J. *J. Am. Chem. Soc.* **1992**, *114*, 5646–5654. (c) Roy, S.; Westmaas, J. A.; Buda, F.; Reedijk, J. *J. Inorg. Biochem.* **2009**, *103*, 1278–1287.
(20) Autschbach, J.; Zheng, S. *Annu. Rep. NMR Spectrosc.* **2009**, *67*, 1–95.
(21) Bühl, M. *Annu. Rep. NMR Spectrosc.* **2008**, *64*, 77–125.
(22) Bühl, M. In *Calculation of NMR and EPR Parameters. Theory and Applications*; Kaupp, M., Bühl, M., Malkin, V. G., Eds.; Wiley-VCH: Weinheim, Germany, 2004; pp 421−431.
(23) Autschbach, J. In *Principles and Applications of Density Functional Theory in Inorganic Chemistry I*; Kaltsoyannis, N., McGrady, J. E., Eds.; Structure and Bonding; Springer: Heidelberg, 2004; Vol. *112*; pp 1−48.
(24) Gilbert, T. M.; Ziegler, T. *J. Phys. Chem. A* **1999**, *103*, 7535–7543.
(25) Autschbach, J.; Zheng, S. *Magn. Reson. Chem.* **2008**, *46*, S48–S55.
(26) Autschbach, J.; Le Guennic, B. *Chem.—Eur. J.* **2004**, *10*, 2581–2589.
(27) Sterzel, M.; Autschbach, J. *Inorg. Chem.* **2006**, *45*, 3316–3324.
(28) Fowe, E. P.; Belser, P.; Daul, C.; Chermette, H. *Phys. Chem. Chem. Phys.* **2005**, *7*, 1732–1738.
(29) Koch, K. R.; Burger, M. R.; Kramer, J.; Westra, A. N. *Dalton Trans.* **2006**, 3277–3284.
(30) Krykunov, M.; Ziegler, T.; van Lenthe, E. *J. Phys. Chem. A* **2009**, *113*, 11495–11500.
(31) Burger, M. R.; Kramer, J.; Chermette, H.; Koch, K. R. *Magn. Reson. Chem.* **2010**, *48*, S38−S47.
(32) Truflandier, L. A.; Autschbach, J. *J. Am. Chem. Soc.* **2010**, *132*, 3472–3483.
(33) Ruden, T.; Ruud, K. In *Calculation of NMR and EPR Parameters*; Kaupp, M., Bühl, M., Malkin, V. G., Eds.; Wiley-VCH: Weinheim, Germany, 2004; pp 153−173.
(34) Mort, B. C.; Autschbach, J. *Chem. Phys. Chem.* **2008**, *9*, 159–170.
(35) Tomasi, J.; Mennucci, B.; Cammi, R. *Chem. Rev.* **2005**, *105*, 2999–3094.
(36) Barone, V.; Improta, R.; Rega, N. *Acc. Chem. Res.* **2008**, *41*, 605–616.
(37) Bühl, M.; Parrinello, M. *Chem.—Eur. J.* **2001**, *7*, 4487–4494.
(38) Bühl, M.; Grigoleit, S.; Kabrede, H.; Mauschick, F. T. *Chem.—Eur. J.* **2006**, *12*, 477–488.
(39) Autschbach, J.; Sterzel, M. *J. Am. Chem. Soc.* **2007**, *129*, 11093–11099.

Our aim is to extend the new insights obtained in ref 32 for platinum anionic complexes to the solution-state ^{195}Pt NMR of the neutral cisplatin complex and three hydroxyl and bromine derivatives, in order to gain a better understanding of ^{195}Pt NMR in aqueous solution in general and of cisplatin-type compounds in particular. On the basis of computations on the set of square-planar platinum(II) complexes *cis*-Pt$(NH_3)_2Cl_2$, *cis*-Pt$(NH_3)_2(OH)Cl$, *cis*-Pt$(NH_3)_2(OH)_2$, and *cis*-Pt$(NH_3)_2Br_2$, we show that whereas the solvent-induced shielding effects for cisplatin and the bromine analogue are rather small, the ^{195}Pt shielding in hydroxyl derivatives reveals strong influences from the hydrogen-bonded network with a sizable long-range order. From a structural point of view, we emphasize the major role of the meso shell, sometimes also called inverse hydration, which has recently also been investigated by Beret and co-workers for oxaliplatin in aqueous solution.[9]

In section 2, the computational protocol as well as technical and methodological aspects are described. Because of the combination of different theoretical methods, this section is relatively long and also reports a subset of the results related to the structural aspects of the solvation shells and the convergence of the platinum shielding constants with the number of solvent molecules. Decomposition of the NMR shifts of the solvated systems into solvent, solute, static, and thermal contributions is discussed in section 3. Structural and NMR results are also presented and discussed within this section. This work concludes with a brief summary of the key findings and an outlook.

2. Methods and Computational Details

2.1. aiMD. Car−Parrinello[40] DFT-based aiMD have been carried out using the Quantum−ESPRESSO suite of programs.[41] The GGA exchange-correlation functional by Perdew, Burke, and Ernzerhof (PBE) has been used[42] in conjunction with ultrasoft pseudopotentials[43] for the atomic cores and a plane-wave basis set for the valence orbitals. Solvation of the platinum complexes has been modeled using cubic simulation boxes with 64 water molecules adapted in size to reach an average density of 1.05 g·cm^{-3}. MD were performed with a fictitious electron mass of 450 au and a time step of 5 au. Ion cores and electrons were both propagated using the velocity Verlet algorithm.[44] Simulations were performed over 5 ps in the *NVT* ensemble prior to 12 ps of production run within the *NVE* ensemble. Additional details regarding aiMD and the platinum pseudopotential along with benchmark verifications of the computational model can be found in ref 32.

In order to probe the reliability of aiMD, radial distribution functions (RDFs), vibrational density of states (VDOS; see the Supporting Information of ref 32), and selected mean distances and angles have been computed for the solute. These calculations have been performed with 4096 MD configurations from the *NVE* ensemble using a sampling period of 2.5 fs. Analyses of the ligand−water RDFs in terms of average nuclear distances and average atomic coordination numbers are reported in Table S1 in the Supporting Information (SI). In the following, the subscript w stands for the hydrogen and oxygen atoms of the water molecules, whereas X refers to the halide atoms of the platinum complexes.

The N···O$_w$ and NH···O$_w$ RDFs show that the first hydration shell of each NH_3 ligand integrates between two and three water molecules with a mean NH···O$_w$ distance of 2.0 Å. This indicates that during the dynamics some water molecules coordinate through hydrogen bonds between the two NH_3 groups or between two hydrogen atoms of the same ammonia ligand. For the platinum halide complexes, the integrations of the first peak of the X···H$_w$ and X···O$_w$ RDFs reveal a halide ligand coordination number above 2.0 with mean X···H$_w$ distances of 2.3 and 2.6 Å for *cis*-Pt$(NH_3)_2Cl_2$ and *cis*-Pt$(NH_3)_2Br_2$, respectively. The results obtained for cisplatin are in agreement with those of previous aiMD studies[10,11] and to a lesser extent with MM MD and MC simulations[7] (see Table S2 in the SI). Comparisons of the VDOS for platinum complexes with available experimental data (from IR and Raman spectroscopy) are compiled in Figures S1−S3 in the SI. Even though the different nature of the samples, solid state for the experiment versus water-solvated for the simulations, prevents an unambiguous assessment of aiMD, we can conclude that the important vibrational eigenmodes involving Pt−ligand motions have been activated during MD simulations. The classical nuclear vibrational motion on the ab initio potential energy surface, from which VDOS is calculated, is, of course, different from the quantized nuclear vibrational motion detected in the experiments, but for the relatively heavy nuclei/groups involved in the vibrations of the platinum complexes, the data are seen to compare quite well. The overall red shift of around 40 cm^{-1} of the peaks in VDOS relative to the experimental frequencies might be related to the usual underestimation of vibrational frequencies with GGA functionals and to the fact that the solvent effects in aiMD simulations are not expected to be identical with the packing effects observed in the solids used for the IR and Raman measurements.

2.2. ^{195}Pt NMR Shielding and Chemical Shift Computations. DFT calculations of the ^{195}Pt NMR shielding have been performed using the Amsterdam Density Functional (ADF) program suite.[45] Relativistic effects were treated by the two-component ZORA,[46,47] using the code developed by Wolff et al.[47] with additional algorithmic developments reported in ref 48. For consistency with our previous studies,[27,32] the revised PBE GGA functional[49] has been used, along with a triple-ζ doubly polarized (TZ2P) Slater-type orbital (STO) basis set for the ligand and solvent atoms and a quadruple-ζ quadruply polarized (QZ4P) STO basis set for platinum.

Liquid-state NMR experiments allow one to determine the strength of NMR shielding of a nucleus through measurement of the isotropic chemical shift (δ). In computational studies, the isotropic shielding constants (σ) for the probe and a reference (ref) nucleus are computed directly. The chemical shift, at a given temperature T, is given by

$$\langle \delta^T \rangle = \frac{\langle \sigma^T_{ref} \rangle - \langle \sigma^T \rangle}{1 - \langle \sigma^T_{ref} \rangle} \quad (1)$$

where the brackets stand for the ensemble average, which we calculate in this work from averages along the aiMD trajectories. Because shielding constants tend to be small, the denominator in eq 1 is usually approximated as $1 - \langle \sigma^T_{ref} \rangle \approx 1$, which makes it particularly easy to convert between different references. For heavy nuclei such as ^{195}Pt, neglecting the reference

(40) Car, R.; Parrinello, M. *Phys. Rev. Lett.* **1985**, *55*, 2471–2474.
(41) Giannozzi, P.; et al. *J. Phys.: Condens. Matter* **2009**, *21*, 395502.
(42) Perdew, J. P.; Burke, K.; Ernzerhof, M. *Phys. Rev. Lett.* **1996**, *77*, 3865–3868.
(43) Vanderbilt, D. *Phys. Rev. B* **1990**, *41*, 7892–7895.
(44) Verlet, L. *Phys. Rev.* **1967**, *159*, 98–103.
(45) Baerends, E. J.; et al. Amsterdam Density Functional, 2010 developers' version, *SCM*; Theoretical Chemistry, Vrije Universiteit: Amsterdam, The Netherlands.
(46) van Lenthe, E.; Baerends, E. J.; Snijders, J. G. *J. Chem. Phys.* **1993**, *99*, 4597–4610.
(47) Wolff, S. K.; Ziegler, T.; van Lenthe, E.; Baerends, E. J. *J. Chem. Phys.* **1999**, *110*, 7689–7698.
(48) Autschbach, J.; Zurek, E. *J. Phys. Chem. A* **2003**, *107*, 4967–4972.
(49) Hammer, B.; Hansen, L. B.; Nørskov, J. K. *Phys. Rev. B* **1999**, *59*, 7413.

shielding in the denominator may lead to differences in the chemical shifts on the order of a percent. The platinum chemical shifts reported in this work have been calculated using eq 1 with respect to the standard reference $[PtCl_6]^{2-}$.

2.3. Time-Averaged ^{195}Pt NMR Shielding Components. In order to determine the best compromise between the statistical efficiency and computational cost for calculation of the aiMD averaged ^{195}Pt shielding, the statistical error of the averaged shielding has been determined as a function of the number of MD configurations used for the averaging. We found that a sampling of 256 uncorrelated configurations over 12 ps of aiMD is sufficient to achieve an acceptable convergence of the platinum shielding, with statistical errors on the order of 20 ppm. Using aiMD for calculation of the time-averaged ^{195}Pt NMR shielding, we have previously proposed to decompose $\langle\sigma^T\rangle$ as[32]

$$\langle\sigma^T\rangle = \langle\sigma^T_{bare}\rangle + \langle\Delta\sigma^T_{solv}\rangle \quad (2)$$

where $\langle\sigma^T_{bare}\rangle$ is equal to the dynamical average of the shielding without any solvent, considering only the bare solute but with nuclear motions as in solution. The solvent correction term $\langle\Delta\sigma^T_{solv}\rangle$ then represents the difference between the aiMD averages with and without explicit solvent, assuming that $\langle\sigma^T\rangle$ is converged with respect to the size of the solvation shell. For simple solvated platinum complexes such as $[PtX_4]^{2-}$, presenting only one type of ligand (X = Cl, Br, CN), which is only an acceptor of hydrogen bonds, we further decompose $\langle\sigma^T_{bare}\rangle$ as[32]

$$\langle\sigma^T_{bare}\rangle = \sigma^T_{av} + \langle\Delta\sigma^T_{vib}\rangle \quad (3)$$

where σ^T_{av} is equal to the shielding obtained from the aiMD-averaged geometry, deduced from one single-point calculation performed with the thermally averaged structure, and $\langle\Delta\sigma^T_{vib}\rangle$ is the "semiclassical" vibrational correction resulting from the classical thermal motion of the nuclei (see ref 32 for further comments on this term). For the cisplatin molecule and the derivatives studied in this work, the shielding decomposition becomes somewhat more delicate. One reason is that, in water at 300 K, the quasi free rotations of the NH_3 and OH groups make it difficult to construct a thermally averaged geometry. Moreover, for bare cisplatin, weak interactions are observed between the ammonia protons and lone pairs of other ligands,[50] whereas in solution, such effects are overpowered by stronger solvent−solute interactions. In order to compute zero-point and temperature-dependent vibrational corrections on the same footing, one needs to use quantum chemical methods, e.g., based on perturbation expansions of vibrational and internal rotation wave functions,[33,34,51] which in our case would have to be adapted to include solvent effects. While it is relatively straightforward to include a polarizable continuum model in such a formalism,[52] we decided to forego that route because our focus is on explicit solvation where hydrogen bonding between the solvent and solute occurs. Then, considering the very good agreement between the skeletal structural parameters of the cisplatin derivatives extracted from aiMD averaging and the ones obtained from a geometry optimization including the implicit treatment of the solvent (see Table S3 of the SI), we have retained this latter set of structures for calculation of σ^T_{av}.

For NMR computations applied to condensed matter, another term neglected in eq 2 is related to the macroscopic magnetic susceptibility of the medium[53] and can be responsible for a solvent-induced shielding on the probe nucleus.[54] For pure liquid water, the macroscopic contribution was estimated to induce a deshielding of −9 ppm,[54] which is very small compared to the chemical shift range of platinum and can be safely neglected at the accuracy level of our computations. Moreover, in our study, both the probe and reference are considered in aqueous solution, in which case the magnetic susceptibility terms cancel in the chemical shifts.

2.4. Treatment of the Solvent Effects. As has been demonstrated in several reviews and articles [for transition metals (TMs), see, for instance, refs 20−23 and references cited therein], the simulation of medium effects on the shielding or the chemical shift of the probed NMR nuclei is greatly improved if the description of the solute−solvent interaction is performed with explicit solvent molecules at the QM level, in particular if there is a possibility for solute−solvent hydrogen-bonding interactions to occur.

Obviously, such types of computations are very demanding in terms of computational resources when the dynamic dimension is included in the spectroscopic property calculations via averages along the MD trajectories. Nevertheless, it is very important to perform such computations based on an explicit dynamic treatment of the solvent effects. It is now possible to probe such solvent effects using first-principles quantum theory and determine exactly how the solvent structure and specific as well as unspecific interactions between the solvent and solute influence the structure and spectroscopic properties of the solvent (or the solution). Moreover, reference data thus created allow one to probe the accuracy of implicit (continuum) solvation models, which are now available within most of the major quantum chemistry packages.[35,55]

Quantum chemical computations are limited by the size of the system to be treated, in terms of the number of basis functions that are needed, which depends on the number of electrons (and therefore the number and type of atoms in the system) and the properties that are of interest. With explicit solvation, while the number of water molecules in aiMD has been kept fixed at 64, our goal has been to include as few explicit solvent molecules as possible in the solvent−cluster NMR calculations. The number n of closest solvent molecules needs to be large enough to reach the boundary distinguishing the solvent shell(s) around the solute from the solute-uncorrelated bulk solvent. In a first approximation, n can be chosen in order to include the first full solvation shell.[32] We note that, for a system presenting a pseudosymmetric first solvation shell, the spherical RDFs appear to be a reliable tool for evaluation of n.

In order to investigate the reliability of an implicit treatment of the solvent effects, we have considered the conductorlike screening model COSMO as implemented self-consistently in ADF.[56−58] Computational settings related to the COSMO model along with a discussion related to the choice of the atomic radius are given in section S3 of the SI.

3. Results and Discussion

The convergence of the ^{195}Pt isotropic shieldings as a function of the number of water molecules surrounding the cisplatin complexes is shown in Figure 1 for *cis*-$Pt(NH_3)_2Cl_2$, *cis*-$Pt(NH_3)_2Br_2$, and *cis*-$Pt(NH_3)_2(OH)_2$. The convergence curves were created based on averages over 256 MD configurations, where the nearest n solvent molecules in each configuration were kept as explicit solvents in the NMR computations. In order to save computational resources, this

(50) Wysokiński, R.; Michalska, D. *J. Comput. Chem.* **2001**, *22*, 901–912.
(51) Ruud, K.; Astrand, P.; Taylor, P. R. *J. Chem. Phys.* **2000**, *112*, 2668–2683.
(52) Kongsted, J.; Ruud, K. *Chem. Phys. Lett.* **2008**, *451*, 226–232.
(53) Mauri, F.; Pfrommer, B. G.; Louie, S. G. *Phys. Rev. Lett.* **1996**, *77*, 5300.
(54) Pfrommer, B. G.; Mauri, F.; Louie, S. G. *J. Am. Chem. Soc.* **2000**, *122*, 123–129.
(55) Cramer, C. J.; Truhlar, D. G. *Chem. Rev.* **1999**, *99*, 2161–2200.
(56) Klamt, A.; Schüürmann, G. *J. Chem. Soc., Perkin Trans. 2* **1993**, 799–805.
(57) Klamt, A. *J. Phys. Chem.* **1996**, *100*, 3349–3353.
(58) Pye, C. C.; Ziegler, T. *Theor. Chem. Acc.* **1999**, *101*, 396–408.

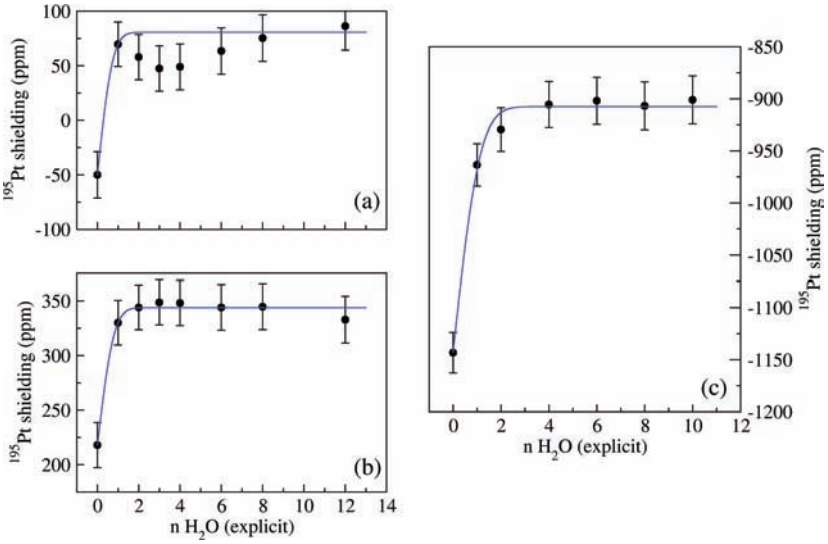

Figure 1. Convergence of the platinum NMR shielding in solvated (a) *cis*-$Pt(NH_3)_2Cl_2$, (b) *cis*-$Pt(NH_3)_2Br_2$, and (c) *cis*-$Pt(NH_3)_2(OH)_2$ complexes as a function of the number of explicit water molecules *n*. Scalar−ZORA calculations. Vertical bars represent the statistical error $\bar{s}$. Each data point involves a sampling of 256 aiMD configurations over 12 ps. Nonlinear curve fits using error functions (cf. ref 32) are represented by blue solid lines.

set of calculations has been carried out at the scalar−ZORA level of theory. Similar to the anionic platinum(II) and platinum(IV) complexes that we studied previously,[32] the convergence of $\langle\sigma^T(^{195}Pt)\rangle$ with respect to *n* can be fitted quite well to an error function or some other type of switching function (see Figure 1). Monotonic solvent number trends have also been observed for MD-averaged NMR observables of small organic molecules (see, for example, refs 59−61). For *cis*-$Pt(NH_3)_2Cl_2$, a nonmonotonic is observed within the range $1 < n < 6$. Closer inspection of the aiMD structures revealed two dative $NH_2{-}H\cdots OH^-$ hydrogen bonds, indicating that for cisplatin a OH^- anion tends to be situated between the two ammonia ligands. Medium-range solvent effects from an increase of *n* beyond 6 overpower these near-range solvent effects. For the other cisplatin derivatives, hydrogen exchange due to transient water protolysis is also found, but only within the second solvent shell. Observation of this phenomenon, which remains a rare event compared to the length of the trajectory, reflects, in a sense, the perturbation of the hydrogen-bond framework of water induced by the presence of the platinum complex. Proton-transfer dynamics have also been reported for the cationic $[Pd(H_2O)_4\cdot H_2O]^{2+}$ and $[Pt(H_2O)_4\cdot H_2O]^{2+}$ complexes.[64,62] Beyond $n < 3$ for Br/Cl and $n < 4$ for the OH derivative, we observe a medium-range regime of solvent effects defined by a plateau, where the metal shielding is only slightly modified as *n* increases. We estimate $\langle\sigma^T(^{195}Pt)\rangle$ to be converged within the statistical errors of the sampling for $n \geq 12$ and 8 for the halide and hydroxy derivatives, respectively. From the Pt···O RDFs plotted in Figure 1 and the corresponding coordination number curves, assuming a spherical solvent shell, *n* can be easily converted to a solvent-shell radius. The boundary of the two regimes is then defined by radii of approximately 4.2 ($n = 3$), 4.3 ($n = 3$), and 4.7 ($n = 4$) Å for *cis*-$Pt(NH_3)_2Cl_2$, *cis*-$Pt(NH_3)_2Br_2$, and *cis*-$Pt(NH_3)_2(OH)_2$, respectively.[63] Compared to inner-shell radii of 5.3 ($n = 12$) and 6.3 ($n \approx 16$) Å obtained previously for $[PtCl_4]^{2-}$ and $[PtBr_4]^{2-}$,[32] this is a significant decrease that we attribute mainly to the lack of negative charges of the complexes studied here.

Further analysis of the Pt···O and Pt···H RDFs reveals the presence of water molecules in the axial region of the neutral square-planar complexes (see Figure 2). The proximity of this water molecule is indicated by the presence of sharp peaks at 2.5 (2.3) Å in the Pt···H RDFs computed for the halide (hydroxy) derivatives (see Figure 2). The first maximum in the Pt···O RDFs, observed around 3.4 Å, supports a "H-ahead" orientation, as shown in the inset of Figure 3. Compared to the anionic square-planar $[PtX_4]^{2-}$ complexes (X = Cl, Br) with oxygen and hydrogen coordination numbers around 2.0, integration of the RDFs yields smaller values of 1.2 (0.6) for oxygen and hydrogen coordination in the halide (hydroxy) cisplatin derivatives. This demonstrates that, on average, only one water molecule is located in the axial coordination region of the complexes.

A suitable model to rationalize this weak axial bonding effect, which is related to phenomena involved in the description of regular hydrogen bonds, is probably the one provided by Beret and co-workers:[64] The Pt···H interaction may be viewed as an ion−dipole interaction (it has also been called "inverse hydration"[65]) involving mainly the occupied non-bonding Pt d_{z^2} valence orbital—the electron-rich center—and the water dipole. The model implies that such a hydration pattern generally can be expected for water-solvated square-planar d^{10} TM complexes independent of the formal charge of the complex. One may expect, however, that the strength

(59) Cossi, M.; Crescenzi, O. *J. Chem. Phys.* **2003**, *118*, 8863.
(60) Benzi, C.; Crescenzi, O.; Pavone, M.; Barone, V. *Magn. Reson. Chem.* **2004**, *42*, S57–S67.
(61) Dračínský, M.; Bouř, P. *J. Chem. Theory Comput.* **2010**, *6*, 288–299.
(62) Beret, E. C.; Pappalardo, R. R.; Doltsinis, N. L.; Marx, D.; Sánchez Marcos, E. *ChemPhysChem* **2008**, *9*, 237–240.
(63) These values can be corrected by taking also into account the H−O distance (1.1 Å) of the water molecule and the van der Waals radius of hydrogen (1.2 Å).
(64) Beret, E. C.; Martínez, J. M.; Pappalardo, R. R.; Sánchez Marcos, E.; Doltsinis, N. L.; Marx, D. *J. Chem. Theory Comput.* **2008**, *4*, 2108–2121.
(65) Kozelka, J.; Bergès, J.; Attias, R.; Fraitag, J. *Angew. Chem., Int. Ed.* **2000**, *39*, 198–201.

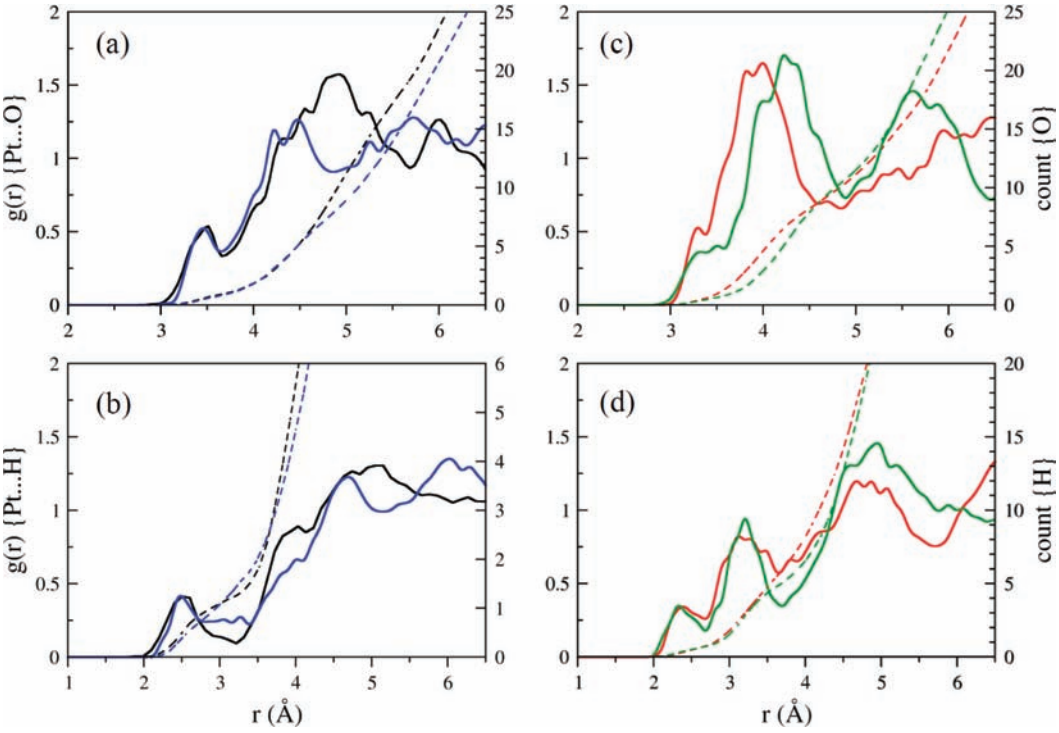

Figure 2. Partial RDFs for Pt···O (a and c) and Pt···H (b and d) atom pairs for the solvated cisplatin systems: *cis*-$Pt(NH_3)_2Cl_2$ (black); *cis*-$Pt(NH_3)_2Br_2$ (blue); *cis*-$Pt(NH_3)_2(OH)_2$ (green); *cis*-$Pt(NH_3)_2(OH)Cl$ (red). The dashed lines give the corresponding coordination number as a function of the distance (right vertical axes).

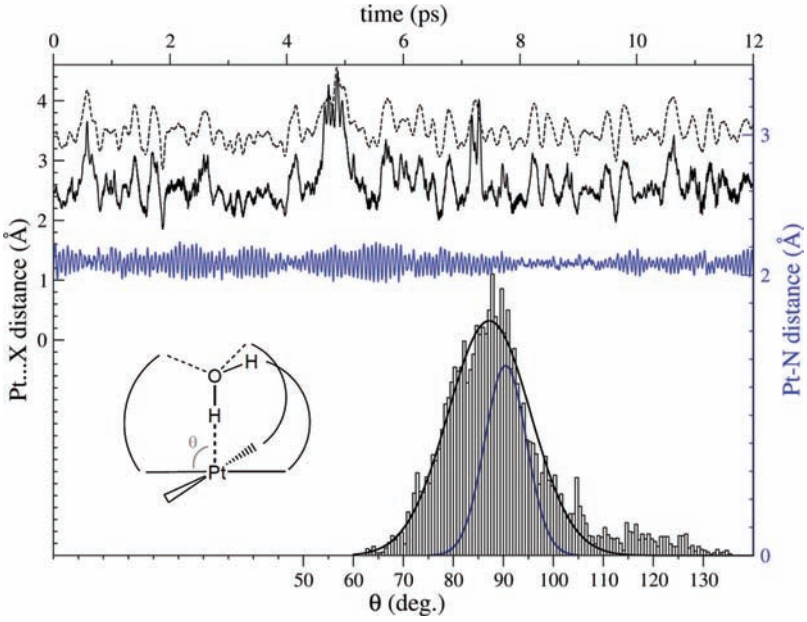

Figure 3. Structural data for the *cis*-$Pt(NH_3)_2Cl_2 \cdot H_2O$ system. In black: Evolution of Pt···H (plain) and Pt···O (dashed) during the aiMD simulation, along with the N−Pt···H angle distribution (histogram and Gaussian fit excluding angles > 105°). In blue: Pt−N distance variation and the N−Pt−N angle distribution (only the Gaussian fit is shown).

of the ion−dipole interaction increases somewhat when going from a cationic to an anionic TM complex. Theoretical investigations based on Hartree−Fock (HF) and post-HF methods and performed on $[Pt(NH_3)_4 \cdot H_2O]^{2+}$ and *trans*-$Pt(NH_3)_2(OH)_2 \cdot H_2O$ systems in the gas phase[65,66] have shown that for the cationic complex a classical hydration, where the water molecule points with its oxygen atom toward the metal center, is energetically competitive, whereas for the neutral complex, the balance is strongly in favor of the inverse-hydration pattern. On the basis of a partitioning of intermolecular potentials,[67] Kozelka et al. argued that the classical hydration is mainly governed by electrostatic and

(66) Bergès, J.; Caillet, J.; Langlet, J.; Kozelka, J. *Chem. Phys. Lett.* **2001**, *344*, 573–577.

(67) Buckingham, A. D.; Fowler, P. W.; Hutson, J. M. *Chem. Rev.* **1988**, *88*, 963–988.

exchange−repulsion interactions, whereas the inverse analogue might be an electron-correlation-driven interaction, which can be rationalized in terms of dispersion effects.[65] Considering the inability of most density functionals to account for pure long-range dispersion effects, GGA exchange−correlation functionals would not be expected to reproduce such interactions. This might be part of the reason why, in a previous aiMD simulation of cisplatin in water with the BLYP functional, the inverse-hydration pattern has not been detected.[10,11] However, we keep in mind that the Pt···H interaction is in close enough range such that electrostatic and orbital overlap effects cannot be excluded as major influences. In a study of solvated oxaliplatin,[9] where the PBE functional has been used (as in the present work), inverse-hydration structures were clearly present in the MD. We also refer the reader to Figure S5 in the SI, where interaction energies between cisplatin and one water molecule in the gas phase are compared at various levels of theory. The PBE curve is seen to be in good agreement with correlated wave-function data, whereas the BLYP functional seems to underestimate the strength of the Pt···H interaction.

According to an investigation of $[Pd(H_2O)_4 \cdot H_2O]^{2+}$ and $[Pt(H_2O)_4 \cdot H_2O]^{2+}$ by Beret et al.,[64] the classical and inverse-hydration interactions involve energies of about 5 kcal·mol^{-1}. In order to fully understand the solvent organization within the axial and equatorial regions of the square-planar platinum complexes, however, an isolated static model is not ideal. The influence of the medium, in our case the presence and dynamics of solvent shells, should also be considered. Indications for the need of a more complex model are given in Figure 3, where the Pt···H, Pt···O, and Pt−N distances for *cis*-$Pt(NH_3)_2Cl_2$ are plotted as a function of time. The Pt···H and Pt···O fluctuations are closely related, with an expected difference of around 1 Å, which is dictated by the geometry and orientation of the water molecule. Superimposed on the Pt···H variation profile are fast small-amplitude oscillations resulting from the intrinsic O−H vibration. Otherwise, the Pt···H and Pt···O distances follow the same variation pattern, indicating that the relative motion between Pt and H is driven by the overall motion of the water molecule that is coupled to the surrounding solvent shell. Comparing the Pt···H and Pt−N profiles, we observe two different regimes, one seemingly random large-amplitude motion that can be attributed to the influence from the surrounding solvent shell and more well-defined Pt−N oscillations with a small-amplitude range. The N−Pt···H and N−Pt−N angle distributions are also plotted in Figure 3. The distribution of N−Pt···H is about twice as wide as that of N−Pt−N and shows a significant probability for angles above 110°. This dissymmetry is correlated to transient departures of the axial water molecule from the metal site to the first solvation shell. These strong fluctuations are also indicated when both the Pt···H and Pt···O distances reach the same value (around 4 Å, at 4.3−4.5 and 6.5−6.7 ps). A more detailed inspection of the hydrogen-bond network around the solute revealed that the inverse-hydration structure and dynamics might be governed by the constitution of a pseudo-3-fold coordination axis oriented along the Pt···O direction (see the inset in Figure 3), with each of the three outer-coordination modes involving, on average, 1.5 solvent molecules. That is, the MD analysis yields indications that the inverse-hydration structural pattern is solvent-assisted. To support this hypothesis, a representative *cis*-$Pt(NH_3)_2Cl_2$ cluster embedded in a network of six solvent molecules has been extracted from MD. Upon geometry optimization of the cluster, the 3-fold outer coordination as well as the inverse water molecule orientation remained intact, with a Pt···H distance of 2.2 Å and a Pt···H−O angle of 175°.[68] Such a static model should not be overinterpreted, considering that during MD water exchange occurs between the bulk and the pseudo-3-fold outer coordination. It appears that additional investigations would be necessary to fully characterize the inverse-hydration structures. This topic will be addressed in a forthcoming article using another NMR probe that is sensitive to bond orders, viz., the *J* coupling.

The importance of inverse hydration has been emphasized in the previous section because the ^{195}Pt NMR shieldings are influenced by this particular interaction. Detailed analyses of the MD data showed that, for cisplatin and the three derivatives, the Pt···H−OH interaction is responsible for a platinum shielding of between 110 and 180 ppm, which represents about three-quarters of the overall solvent effect. For $[PtX_4]^{2-}$ systems, we found previously that the contribution of the nearest two water molecules yields about half of the total solvent effect. Thus, these nearest water molecules need to be included explicitly in quantum mechanical (QM) computations of the average NMR shielding in solution. Moreover, as pointed out above, a reliable modeling of the solvent effect on the ^{195}Pt NMR shieldings in cisplatin derivatives should include additional solvent molecules, i.e., $n > 3$ ($n > 4$ for the hydroxy derivative), and ideally the model should afford one full first solvation shell to achieve reasonably well-converged results.

On the basis of eqs 2 and 3, the ^{195}Pt shielding contributions from the average geometry effects in solution, vibrational effects, and solvent effects, i.e., σ^T_{av}, $\langle\Delta\sigma^T_{vib}\rangle$, and $\langle\Delta\sigma^T_{solv}\rangle$, respectively, are compiled in Table 1 and graphically displayed in Figure 4, along with the sum of $\langle\Delta\sigma^T_{vib}\rangle + \langle\Delta\sigma^T_{solv}\rangle$ and the statistical errors. These computations have been performed at the spin−orbit ZORA level of theory using 256 aiMD configurations, with 12 and 10 surrounding water molecules for the halide and hydroxy derivatives, respectively.[69] The vibrational deshielding effects are seen to counterbalance the solvent-induced shieldings, which, for the hydroxy derivative, reach 288 ppm. For cisplatin and the bromine derivative, the solvent effects are weaker, 140 and 84 ppm, respectively. The decrease of the solvent effects from chlorine to bromine is consistent with our previous findings on $[PtX_n]^{2-}$ systems[32] and with the fact that the strongest solute−water interactions, a perturbation from the NMR point of view involving mainly hydrogen bonds for the protic solvent, are expected to be somewhat weaker for bromine. The hydroxy cisplatin derivatives represent strong hydrogen-bond donor/acceptors, and accordingly the solute−water interactions are significant, resulting in sizable solvent-induced shieldings. Statistical errors for the vibrational contributions are shown separately in Figure 4 [for brevity, they are reported only for the aiMD−explicit approach; these terms should not be confused with the total statistical errors ($\bar{s}$) in Table 1]. As discussed in section 2.3, evaluation

(68) Calculations performed with the PBE functional and at the MP2 level of theory yielded similar results.

(69) To give the reader an idea about the computational effort, at this level of theory each configuration required less than 4 h on a system with dual 3.2 GHz Intel Xeon processors. With a scalar−ZORA approach, the computational time is reduced to less than 20 min.

Table 1. Decomposition of the aiMD-Averaged ^{195}Pt Isotropic Shielding Following Equations 2 and 3 Using 12 Water Molecules for the Halide Complexes and 10 for the Hydroxo Complexes Based on 256 aiMD Configurations (see Figure 1) and Spin−Orbit ZORA Computations[a]

	dynamic					static
complex	σ_{av}^{T} [b]	$\langle\Delta\sigma_{vib}^{T}\rangle$	$\langle\Delta\sigma_{solv}^{T}\rangle$	sum $\pm$ $\bar{s}$ [c]	dev[d] $\langle\sigma_{cosmo}^{T}\rangle$	dev[a] σ_{cosmo}
cis-Pt$(NH_3)_2Cl_2$	3532	−129	140	3672 ± 16	14	203
cis-Pt$(NH_3)_2Br_2$	3946	−83	84	4031 ± 15	−32	89
cis-Pt$(NH_3)_2$(OH)Cl	3081	−239	253	3334 ± 15	−21	256
cis-Pt$(NH_3)_2(OH)_2$	2737	−174	288	3025 ± 15	11	249
$[PtCl_6]^{2-}$ [e]	1274	−66	302	1576 ± 38	38	74
absolute mean dev					23	174

[a] Also listed are deviations between the explicitly solvated MD results and aiMD averages using COSMO (no explicit solvation) and COSMO single-point calculations. [b] Shielding components arising from decomposition given in eqs 2 and 3. [c] Sum of the contributions along with the statistical error $\bar{s}$. [d] Deviations calculated with respect to the aiMD averaging including the explicit solvent treatment. [e] From ref 32; reference used for calculation of the ^{195}Pt chemical shifts.

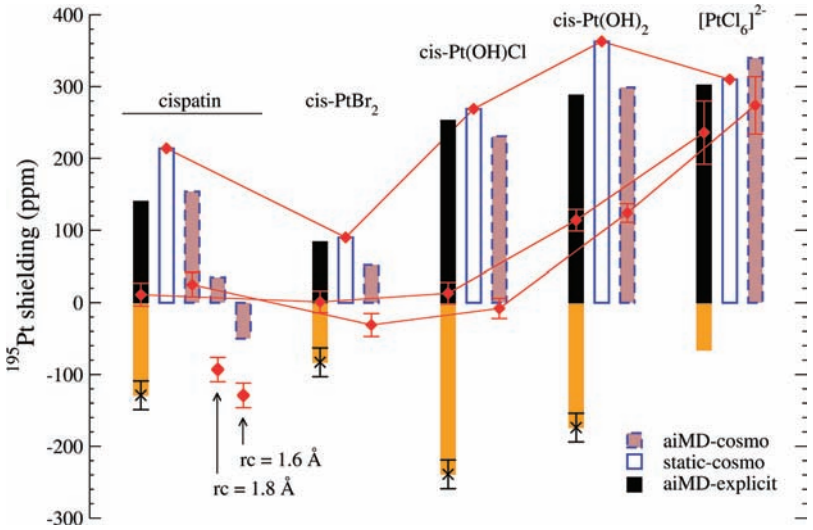

Figure 4. Solvent (black) and vibrational (orange) contributions ^{195}Pt isotropic shielding in cisplatin derivatives and $[PtCl_6]^{2-}$. Spin−orbit ZORA computations. The sums of the contributions are indicated by the red diamonds, along with the corresponding standard deviations (error bars). The black crosses indicate standard deviations determined separately for the vibrational contributions in the MD averages performed with explicit solvation. Also shown are the results for cisplatin from COSMO calculations with different platinum radii (rc). For a direct comparison, the zero of the vertical axis has been set to σ_{av}^{T}, given in Table 1 for each system.

of $\langle\Delta\sigma_{vib}^{T}\rangle$ using eq 3 requires σ_{av}^{T}. We found that σ_{av}^{T} variations, arising from weak intermolecular interactions occurring between the NH_3 and OH hydrogen atoms and the other ligand lone pairs in the absence of solvent molecules, oscillate by ±20 ppm; they are of the same order as the statistical errors. For the halide derivatives and *cis*-Pt$(NH_3)_2$(OH)Cl, the sums $\langle\Delta\sigma_{vib}^{T}\rangle + \langle\Delta\sigma_{solv}^{T}\rangle$ cancel almost exactly. Because of this cancellation, for these three platinum complexes, the overall shielding variations are dominated by σ_{av}^{T}.

With the explicit solvation reference values (referred to as "aiMD−explicit" in the following) at hand, it is now interesting to probe the reliability of an implicit solvent model. For this purpose, the aiMD−NMR averaging protocol has been applied to the platinum complexes by substituting the explicit water molecules by the COSMO model (aiMD−COSMO), using the parameters given in section S3 in the SI. For comparison, single-point NMR calculations of the ^{195}Pt shieldings on a COSMO-optimized geometry, the same geometries as those used for computation of σ_{av}^{T}, have also been performed with and without COSMO (referred to as static−COSMO). As highlighted in section S3 in the SI, the ^{195}Pt shieldings in principle require an optimization of the platinum COSMO radius. The significance of this parametrization is reinforced by the conclusions arising from RDF analysis (see Figures 2 and 3 and the discussion of the data). We found that for a radius of 2.1 Å the agreement with the aiMD−explicit reference values is satisfactory (vide infra). Data in Figure 4 show that the solvent-induced shielding obtained with COSMO for platinum radii of 1.8 and 1.6 Å, respectively, is underestimated by 104 and 190 ppm. In the latter case, the solvent effects even lead to a deshielding of the metal center. The physical interpretation of this unexpected effect might lie in the inverse-hydration pattern previously identified, which may not be described well with a purely electrostatic model such as COSMO.

Somewhat unexpectedly, when using the optimized COSMO radius of 2.1 Å for platinum, the aiMD−COSMO solvent shieldings overall match fairly well with the aiMD−explicit results, with a mean absolute deviation of about 23 ppm (see Table 1). In the static−COSMO approach, the discrepancy is between 74 ppm for $[PtCl_6]^{2-}$ and 256 ppm for *cis*-Pt$(NH_3)_2$(OH)Cl (see Figrue 4). One major shortcoming of the static approach lies obviously in the neglect of the deshielding vibrational contributions, which leads to a sizable mean deviation of 174 ppm on the ^{195}Pt shielding values between the two approaches (see Table 1) and varies strongly from one complex to another. The question arises whether these effects also influence the *relative* chemical shifts, given

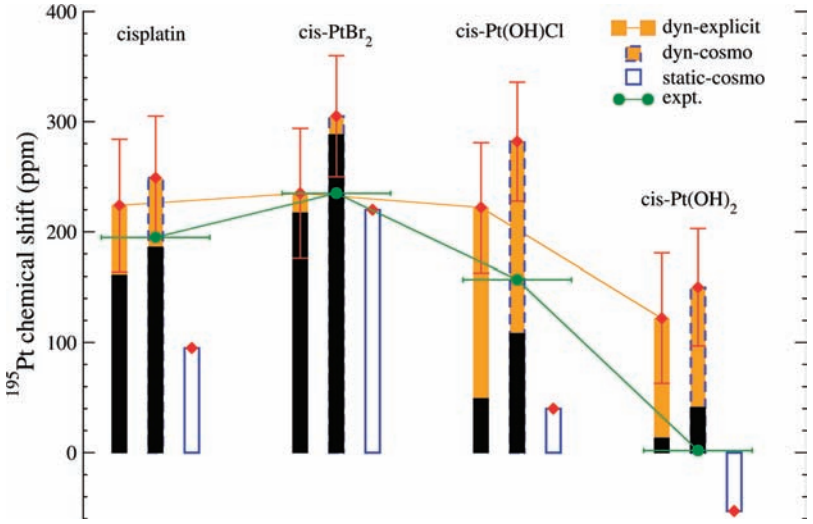

Figure 5. Solvent and vibrational contributions to the ^{195}Pt chemical shift in cisplatin and cisplatin derivatives. Spin−orbit ZORA calculations. See also the caption of Figure 4. For a direct comparison, the zero of the vertical axis has been set to δ^{T}_{av}, given in Table 2 for each system.

Table 2. Decomposition of the aiMD-Averaged ^{195}Pt Chemical Shifts Calculated at the Spin−Orbit ZORA Level of Theory, Explicit Treatment of the Solvent, and Deviation between the aiMD-Averaged Data and aiMD−COSMO and Static−COSMO Results (See Also Figure 5)

	dynamic						static		
complex	δ^{T}_{av}	$\Delta\langle\delta^{T}_{vib}\rangle$	$\Delta\langle\delta^{T}_{solv}\rangle$	sum $\pm\ \bar{s}^{b}$	$\langle\delta^{T}_{cosmo}\rangle$	dev[c]	δ_{cosmo}	dev[c]	expt[a]
cis-Pt$(NH_3)_2Cl_2$	−2324	63	161	−2100 ± 54 (2%)	−2075	24 (3%)	−2229	−129 (−4%)	−2139
cis-Pt$(NH_3)_2Br_2$	−2694	18	217	−2459 ± 53 (0%)	−2389	70 (3%)	−2473	−15 (−1%)	−2459
cis-Pt$(NH_3)_2$(OH)Cl	−1983	174	49	−1761 ± 53 (4%)	−1701	60 (7%)	−1943	−182 (−6%)	−1826
cis-Pt$(NH_3)_2(OH)_2$	−1574	109	13	−1452 ± 53 (8%)	−1424	28 (10%)	−1627	−175 (−3%)	−1572
mean dev				(4%)		45 (6%)		−125 (−4%)	

[a] For *cis*-Pt$(NH_3)_2Br_2$ and *cis*-Pt$(NH_3)_2$(OH)Cl, see ref 70. For *cis*-Pt$(NH_3)_2(OH)_2$, see refs 71 and 72. For *cis*-Pt$(NH_3)_2Cl_2$, see the mean value from refs 19, 70, and 73. [b] Sum of the contributions along with the statistical error $\bar{s}$. [c] Deviations calculated with respect to the aiMD averaging including the explicit solvent treatment. The deviation relative to experiment is given in parentheses.

the well-known error cancellations previously discussed for other platinum complexes.[27] In order to further analyze the platinum chemical shifts calculated with the three approaches, eqs 1−3 have been combined to identify the average structure, vibrational, and solvent contributions to the chemical shifts, i.e., δ^{T}_{av}, $\Delta\langle\delta^{T}_{vib}\rangle$, and $\Delta\langle\delta^{T}_{solv}\rangle$, respectively. The results are shown in Figure 5 along with the statistical errors (see Table 2 for numerical data). First, consider the aiMD−explicit results. It is important to keep in mind that the large solvent and vibrational effects on the shielding of the reference compound (around 240 ppm; see Figure 4) contribute to the chemical shifts. The medium-induced chemical shifts in the hydroxy derivatives can be viewed mainly as nuclear-motion-driven, whereas for halide complexes, we observe a predominance of solvent−solute electronic interactions. Overall, for the aiMD−explicit approach, the chemical shifts deviate from experiment by 4% on average (see Table 2), which constitutes a very acceptable agreement. The dynamic averaging with COSMO also performs well provided that the platinum radius is well chosen. Compared to the aiMD reference values, the static−COSMO approach reveals shortcomings, but the experimental values lie between the aiMD−explicit and static−COSMO results and therefore the overall deviations from experiment are also relatively small with the static−COSMO approach. This good performance arises partially because in the aiMD averages there are important contributions to the platinum shielding constants that cancel each other quite effectively (see Figure 4).

An assessment of the reliability of each model with respect to liquid-state experimental values (see Table 2 and Figure 5) must be made cautiously. Besides the challenges associated with a good description of the medium effects, the calculations afford inaccuracies arising from the usual quantum theoretical approximations. These are in our case mainly the approximate treatment of the electron correlation by DFT, basis set incompleteness, and the approximate nature of the relativistic Hamiltonian. These approximations are necessary in order to allow a detailed microscopic description of the NMR chemical shifts in solution at an affordable computational effort. It is likely that at the level of theory employed in this work the exchange−correlation functional is the main influence limiting the accuracy of the results. Overall, only a 4% average deviation from experiment should be considered as a significant step forward with the challenging task of describing heavy-metal

(70) Appleton, T. G.; Hall, J. R.; Ralph, S. F. *Inorg. Chem.* **1985**, *24*, 4685–4693.
(71) Appleton, T. G.; Berry, R. D.; Davis, C. A.; Hall, J. R.; Kimlin, H. A. *Inorg. Chem.* **1984**, *23*, 3514–3521.
(72) Boreham, C.; Broomhead, J.; Fairlie, D. *Aust. J. Chem.* **1981**, *34*, 659–664.
(73) Ismail, I. M.; Sadler, P. J. In *Platinum, Gold, and Other Metal Chemotherapeutic Agents*; Lippard, S. J., Ed.; ACS Symposium Series; American Chemical Society: Washington, DC, 1983; pp 171−190.

chemical shifts in solution using first-principles theory because it requires one to treat both the reference and the probe complexes—which, as in our case, have different solvent-shell structures—similarly well.

Instead of considering relative deviations of the chemical shifts from experimental data, which depend on the choice of the reference compound, one may alternatively consider deviations between theory and experiment relative to the chemical shift range of platinum(II), which covers about 4000 ppm.[16] In this case, the average deviations for the explicitly solvated dynamic model from experiment are only on the order of 1%. For the static−COSMO approach, the agreement with experiment is seen to be to some degree a result of error cancellation. Thus, it should be investigated if a similarly good performance of this solvent model will be found for other types of complexes and other NMR parameters.

4. Concluding Remarks

Within the GGA DFT framework, we have demonstrated that the combination of Car−Parrinello aiMD with the spin−orbit ZORA relativistic NMR calculations allows one to accurately predict ^{195}Pt NMR chemical shifts of cisplatin derivatives in aqueous solution, with less than 5% deviation from experiment. The results further validate the computational model used here, which was initially devised in ref 32. In a forthcoming paper, we further validate the computational protocol for Pt-N spin-spin coupling constants.[74]

The solvent structures around the neutral platinum complexes studied in this work differ in various aspects from those of the anionic platinum halide complexes that we investigated in ref 32. One of the important dynamic features appears to be the inverse-hydration coordination pattern, which has also previously been reported in other MD studies. Our analysis indicated that this structural pattern is to some extent solvent-assisted. Given the explicit treatment of the solvent effect as a reference, an implicit solvation model such as COSMO is able to recover the main solvent-induced NMR contributions with good reliability only if the dynamic averaging is included in the calculations. For the complexes studied here, the good performance relies on a cancellation of sizable solvent and vibrational effects on the metal shielding.

Improved results might be obtained when switching to hybrid functionals, although for platinum and other heavy-metal shifts a recent benchmark study using static structures reported no significant improvements with the B3LYP hybrid functional.[30] For a fair assessment and given the importance of a detailed microscopic description of the dynamic solvent structure around the complexes, it would be important to compare different functionals both in MD and in NMR computations. Considering the speed-ups achieved in the past decades for NMR computations of metal complexes, both from an algorithmic point of view and because of the wide availability of affordable fast computer hardware, and considering the ease with which relativistic DFT methods can now be applied to such problems, it is foreseeable that dynamic averaging of the NMR parameters including an explicit solvent shell is going to become a routine task in the not too distant future. An interesting problem in this context remains to treat the nuclear motion at some quantum theoretical level in order to incorporate, for instance, zero-point vibrational effects in the calculated results.

An extension of this work to liquid-phase ^{195}Pt NMR simulations of cisplatin binding to DNA oligonucleotides might be feasible by spending considerable computational effort on full QM models or by applying approximations that limit the number of electrons to be treated by QM and use MM force fields for large parts of the system. For instance, when using hybrid QM/MM MD schemes for the phase space sampling, based on the results of this work, one can speculate that for NMR computations a truncation of the explicit QM part within a radius of about 5 Å around the metal center would be sufficient to reach accurate DFT predictions. Naturally, a reliable model needs to account for the platinum coordination sphere being properly reconstructed using adequate boundary substituents. It would also be highly important to allow for sufficient MD sampling time in order to properly characterize the dynamics of the damaged region of the DNA.

Acknowledgment. The authors are grateful for financial support from the National Science Foundation (Grants CHE 0447321 and 0952253) and acknowledge support from the Center for Computational Research at the University at Buffalo for the research reported here.

Supporting Information Available: RDFs and VDOSs for the complexes, tabulated data derived from the RDFs, and a comparison of the interaction energies between cisplatin and water using different levels of theory. This material is available free of charge via the Internet at http://pubs.acs.org.

(74) Sutter, K.; Truflandier, L. A.; Autschbach, J. *ChemPhysChem*, in press.